*Human Molecular Genetics, 2012, Vol. 21, No. 8* ***1744–1759***
*doi:10.1093/hmg/ddr608*
*Advance Access published on December 30, 2011*

# Impaired neural development in a zebrafish model for Lowe syndrome

**Irene Barinaga-Rementeria Ramirez[1], Grzegorz Pietka[1], David R. Jones[2], Nullin Divecha[2], A. Alia[3], Scott C. Baraban[4], Adam F. L. Hurlstone[1] and Martin Lowe[1,*]**

[1]Faculty of Life Sciences, University of Manchester, The Michael Smith Building, Oxford Road, Manchester M13 9PT, UK, [2]CRUK Inositide Laboratory, The Paterson Institute for Cancer Research, Manchester, UK, [3]Leiden Institute of Chemistry, Leiden University, 2300 RA Leiden, The Netherlands, and [4]Department of Neurological Surgery, University of California San Francisco, San Francisco, CA 94143, USA

Received October 25, 2011; Revised and Accepted December 21, 2011

**Lowe syndrome, which is characterized by defects in the central nervous system, eyes and kidneys, is caused by mutation of the phosphoinositide 5-phosphatase OCRL1. The mechanisms by which loss of OCRL1 leads to the phenotypic manifestations of Lowe syndrome are currently unclear, in part, owing to the lack of an animal model that recapitulates the disease phenotype. Here, we describe a zebrafish model for Lowe syndrome using stable and transient suppression of OCRL1 expression. Deficiency of OCRL1, which is enriched in the brain, leads to neurological defects similar to those reported in Lowe syndrome patients, namely increased susceptibility to heat-induced seizures and cystic brain lesions. In OCRL1-deficient embryos, Akt signalling is reduced and there is both increased apoptosis and reduced proliferation, most strikingly in the neural tissue. Rescue experiments indicate that catalytic activity and binding to the vesicle coat protein clathrin are essential for OCRL1 function in these processes. Our results indicate a novel role for OCRL1 in neural development, and support a model whereby dysregulation of phosphoinositide metabolism and clathrin-mediated membrane traffic leads to the neurological symptoms of Lowe syndrome.**

## INTRODUCTION

Oculocerebrorenal syndrome of Lowe is an X-linked disorder with the hallmark symptoms of congenital cataracts, mental retardation and proximal renal tubulopathy (1,2). Lowe syndrome is caused by mutation of the gene encoding OCRL1, a type II inositol polyphosphate 5-phosphatase which preferentially hydrolyses PtdIns(4,5)$P_2$, although it also displays activity towards PtdIns(3,4,5)$P_3$ (3,4). Mutation of OCRL1 also causes Dent disease (in ~20% of cases), which primarily affects the kidneys with little or none of the associated ocular and neurological symptoms (5,6).

OCRL1 is a multi-domain protein with an N-terminal PH domain, a central 5-phosphatase domain and C-terminal ASH and catalytically inactive RhoGAP-like domains (4,7,8). OCRL1 is localized to the trans-Golgi network, early endosomes, lamellipodia and clathrin-coated membrane-trafficking intermediates (4). It has also recently been localized to cellular junctions and the intercellular bridge during cytokinesis (9,10). Targeting at these various locations is mediated through binding with Rab GTPases (11,12), although interaction with other proteins helps localize the protein to particular membrane domains. Enrichment in clathrin-coated trafficking intermediates is dependent upon binding to components of the clathrin machinery (clathrin heavy chain and the α-adaptin subunit of AP2) (8,13–15), while interaction with the small GTPases Rac1 and Cdc42 likely helps OCRL1 associate with the actin cytoskeleton (7,16,17). OCRL1 also binds the ARF1 and ARF6 GTPases (18), the signalling adaptor protein APPL1 (7,19) and the endosomal proteins IPIP27A and B (or Ses1 and 2) that were recently shown to participate in endocytic recycling (20,21).

Functional studies using tissue culture cells have revealed a role for OCRL1 in endosomal trafficking (14,22,23) consistent

*To whom correspondence should be addressed. Tel: +44 1612755387; fax: +44 1612751505; Email: martin.lowe@manchester.ac.uk

with binding to components of the endocytic trafficking machinery. Analysis of Lowe syndrome patient cells has also revealed defective cell adhesion and migration upon loss of OCRL1 function (9,24). These may correspond to a direct effect upon the actin cytoskeleton or could arise through altered trafficking of the machinery required for these processes. A role for OCRL1 in cytokinesis has also recently been discovered, where OCRL1 would appear to act directly given its localization to the intercellular bridge prior to abscission (10,25). OCRL1 likely regulates these processes through PtdIns(4,5)$P_2$ and PtdInd(3,4,5)$P_3$ hydrolysis, which in turn controls membrane and actin dynamics at specific subcellular locations.

Vertebrates express a second 5-phosphatase that is closely related to OCRL1 called INPP5B (26,27). INPP5B shares the same domain organization and has a similar substrate preference to OCRL1, and is also localized to the Golgi apparatus and endosomes (7,8,27–29). INPP5B binds to many of the OCRL1-binding partners, although there are some differences, most notably in clathrin binding, which is lacking in INPP5B (7,29). It appears that OCRL1 and INPP5B share overlapping functionality, since knockout of OCRL1 or INPP5B in mice gives no phenotype, or in the case of INPP5B, a very mild one restricted to the testis, while double-knockout of OCRL1 and INPP5B results in early embryonic lethality (30,31). This suggests that mouse INPP5B can fully compensate for OCRL1, while in humans, compensation is only partial. In support of this hypothesis, a mouse model in which human INPP5B is expressed in a background lacking murine OCRL1 and INPP5B exhibits a renal tubulopathy reminiscent to that seen in Lowe syndrome patients (32). The ability of INPP5B to compensate for loss of OCRL1 likely explains the tissue-specific nature of Lowe syndrome, despite the near-ubiquitous expression of OCRL1 in human tissues.

Despite progress in the understanding of the cell biology of OCRL1, how loss of the protein leads to the pathological changes seen in Lowe syndrome and Dent disease remains unclear. It has been proposed that defective trafficking of the multi-ligand receptor megalin accounts for the renal symptoms observed in these disorders, but this remains to be demonstrated (4,33). The basis for the neurological symptoms of Lowe syndrome is even less well understood. These include mental retardation, neonatal hypotonia, stereotypical behaviour and an increased susceptibility to seizures (2). Magnetic resonance imaging (MRI) indicates cystic lesions in the white matter of Lowe syndrome patients, often in the periventricular region (2,34–36). It is interesting to note that OCRL1 is highly expressed in brain, and that only the longer splice variant, isoform a, is present in this tissue, while other tissues express both isoforms a and b (37,38). OCRL1 isoform a exhibits higher affinity clathrin-binding and increased association with clathrin-trafficking intermediates (15), suggesting an important role for OCRL1 in clathrin-mediated trafficking in the brain. This hypothesis remains to be tested.

In this study, we describe a zebrafish model for Lowe syndrome. OCRL1-deficient zebrafish embryos are more susceptible to seizures and adults exhibit cystic brain lesions, recapitulating the symptoms of Lowe syndrome. Loss of OCRL1 impairs cell survival and reduces cell proliferation within the developing neurological tissue, indicating a novel role for OCRL1 in embryonic brain development. Both catalytic activity and clathrin-binding are required for OCRL1 function during this process, suggesting that dysregulation of phosphoinositide metabolism and clathrin-mediated trafficking are responsible for the neurological symptoms of Lowe syndrome.

## RESULTS

### Conservation of OCRL1 and INPP5B in vertebrates

Genes encoding the paralogues OCRL1 and INPP5B are present in all vertebrates, including the zebrafish *Danio rerio*, while 'lower' metazoans such as *Drosophila melanogaster* and *Caenorhabditis elegans* express only a single orthologue of these proteins (Supplementary Material, Fig. S1). Zebrafish has a single gene for each of the phosphatases, with OCRL1 mapping to chromosome 14 and INPP5B to chromosome 16. There is a high degree of sequence conservation between zebrafish OCRL1 and INPP5B and their human orthologues (Fig. 1A). The functional domains of both proteins are also well conserved, as are the interaction motifs for the known binding partners of these proteins, including the two clathrin boxes present in the PH and RhoGAP-like domains of OCRL1 (Fig. 1A and Supplementary Material, Fig. S2).

### Zebrafish OCRL1 is localized to the Golgi apparatus and early endosomes

To determine the subcellular localization of zebrafish OCRL1, a GFP-tagged version was expressed in cultured zebrafish fibroblasts and immunofluorescence microscopy performed. GFP–OCRL1 fluorescence coincided with staining of the Golgi marker golgin-84 and the early endosome marker EEA1 (Fig. 1B). We also observed colocalization with co-transfected mCherry-tagged clathrin light chain (CLC) in cytoplasmic puncta, consistent with the presence of zebrafish OCRL1 in clathrin-coated trafficking intermediates (Fig. 1B). Isoform b was also present at the Golgi apparatus and endosomes, but the cytoplasmic puncta were less apparent, as seen with the human protein, suggesting reduced association with clathrin structures. This was confirmed by quantitation, which revealed that 37% of clathrin puncta contained OCRL1 isoform a while only 13% were positive for isoform b. These results indicate that zebrafish OCRL1 exhibits a similar subcellular distribution to the human protein.

### Expression profile and splicing of zebrafish OCRL1

We next analysed the expression of zebrafish OCRL1 in adult tissues by reverse transcriptase-polymerase chain reaction (RT-PCR) and western blotting. OCRL1 mRNA was detected in all adult tissues examined, indicating its widespread expression (Fig. 1C). Using primers to discriminate between OCRL1 splice isoforms, we found that isoform b is the predominant form in most tissues, while in heart and skeletal muscle, isoform a is more abundant and in brain it is the only splice

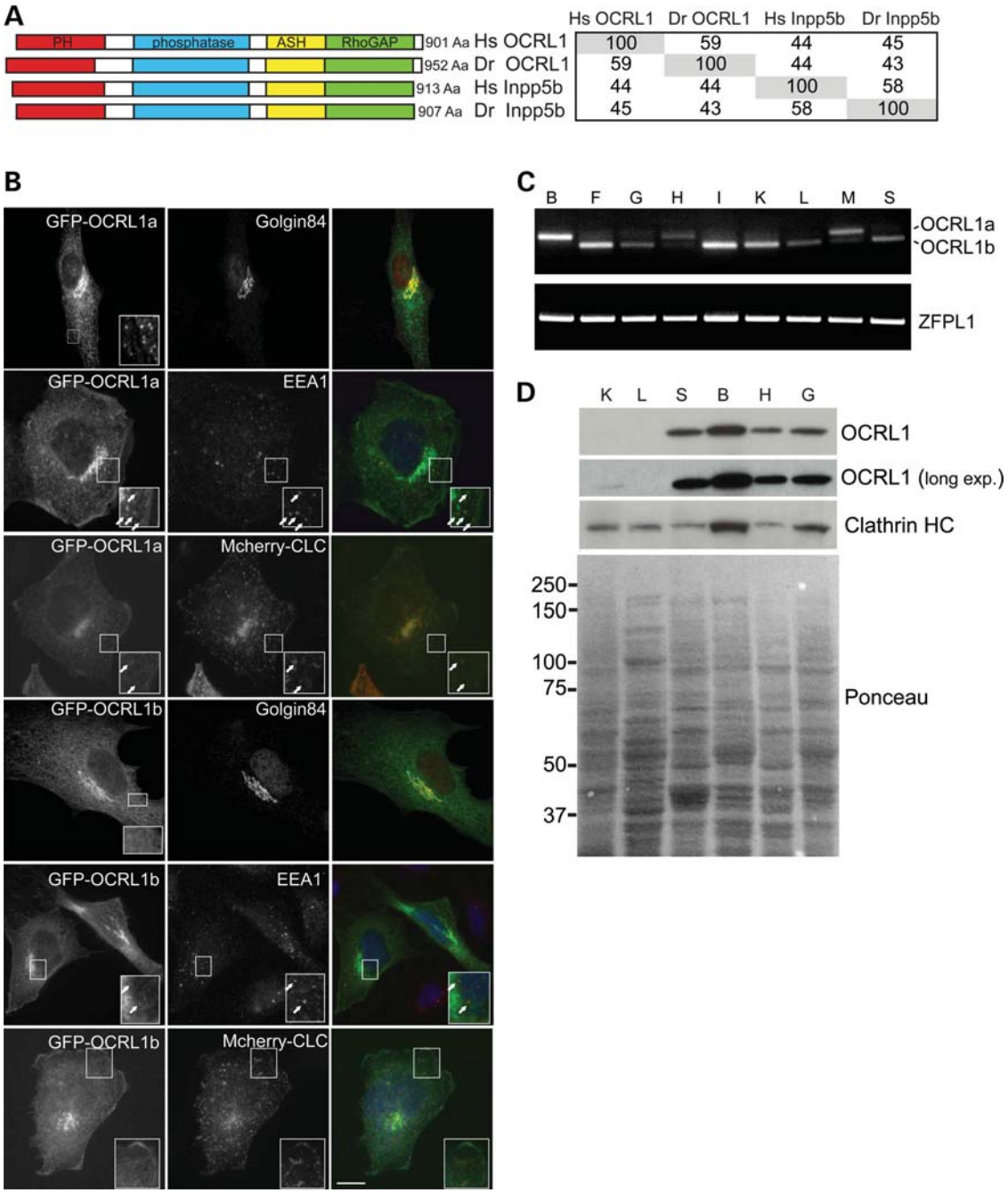


**Figure 1.** OCRL1 domain organization, subcellular localization, and tissue-specific splicing and expression are conserved in zebrafish. (**A**) Schematic view of human and zebrafish OCRL1 and Inpp5 showing the predicted PH, 5-phosphatase, ASH and RhoGAP-like domains. The table indicates amino acid identity between the proteins. (**B**) Immunofluorescence microscopy of zebrafish AB9 or PAC2 fibroblast cells expressing GFP-tagged OCRL1 isoform a or b (green) with or without mCherry-tagged clathrin light chain (CLC) and labelled with antibodies to Golgin84 or EEA1 (red). Arrows indicate colocalization of OCRL1a with EEA1 or mCherry-clathrin light chain. Scale bar, 10 μm. (**C**) RT–PCR of adult zebrafish tissues using primers against OCRL1 isoform a and b, or the control ZFPL1. B, brain; F, fin; G, gill; H, heart; I, intestine; K, kidney; L, liver; M, muscle; S, skin. (**D**) Western blot of zebrafish adult tissues using the indicated antibodies. K, kidney; L, liver; S, skin; B, brain; H, heart; G, gill. Ponceau staining of the membrane shows similar loading per lane.

isoform expressed. This expression profile is identical to that seen with human OCRL1 (38). As shown in Fig. 1D, OCRL1 was most abundant at the protein level in the brain, similar to that seen with the mouse protein (30). We could also detect OCRL1 in other tissues, although its abundance in liver and kidney appeared low (Fig. 1D).

The expression of OCRL1 during embryogenesis was also analysed. RT–PCR indicated the presence of maternal OCRL1 mRNA at the onset of development, with zygotic expression evident throughout subsequent developmental stages (Fig. 2A). Western blotting confirmed the expression of OCRL1 protein throughout the early stages of development

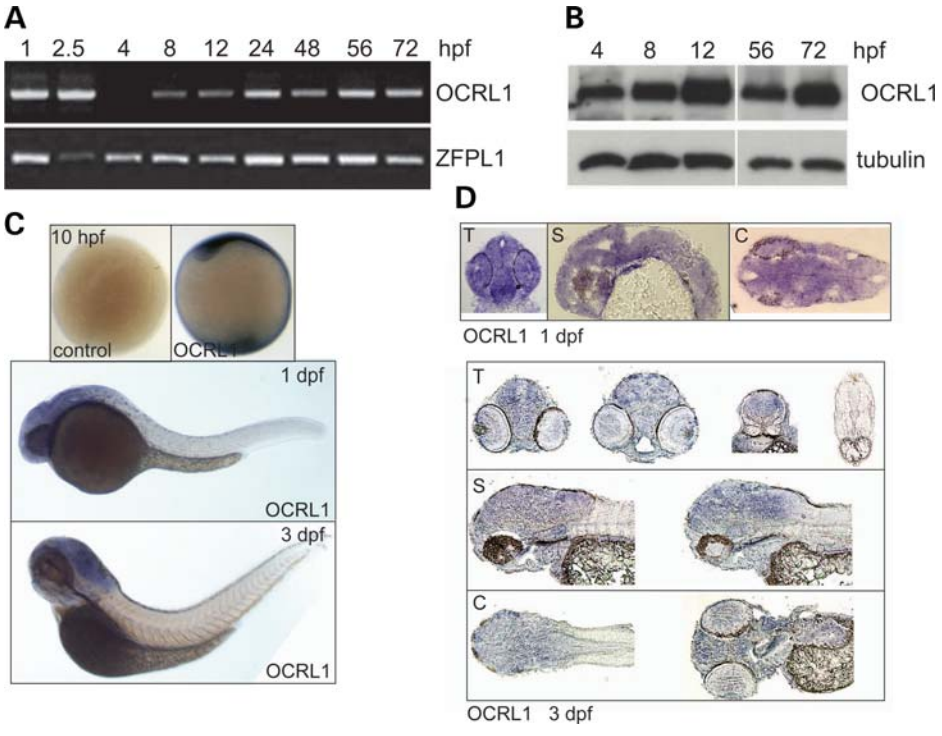


**Figure 2.** Developmental expression of zebrafish OCRL1. (**A**) RT–PCR of cDNA prepared at different embryonic developmental time points using primers against total OCRL1 and the control ZFPL1. (**B**) Western blotting of protein extracts from zebrafish embryos at different developmental time points with the indicated antibodies. (**C**) Images of whole-mount ISH with OCRL1 probe antisense and sense (control) at the developmental time-points indicated. (**D**) Transverse (T), sagittal (S) and coronal (C) cryosections of whole-mount ISH with OCRL1 probe at the times of development indicated.

(Fig. 2B). Whole-mount *in situ* hybridization revealed that OCRL1 expression is ubiquitous, with enrichment seen in the neural tissue at 1 and 3 days post-fertilization (dpf) (Fig. 2C). This staining is specific: we observed identical patterns with two independent probes and there was no staining with the sense control probes at all stages analysed (Fig. 2C and data not shown). Analysis of cryosections indicates that OCRL1 is widely expressed throughout the neural tissue, with no particular enrichment in any region of the brain (Fig. 2D).

## OCRL1-deficient embryos have elevated levels of PtdIns(4,5)$P_2$

To generate a vertebrate model for Lowe syndrome in which we could analyse both embryogenesis and later stages of life, we obtained transgenic zebrafish containing a retroviral insertion in the OCRL1 promoter (Fig. 3A, left). Genotyping confirmed the presence of the insertion upstream of the OCRL1 start codon (Fig. 3A, right). Western blotting of homozygous mutant embryos indicated that protein expression was reduced by approximately 70% in this line, herein referred to as OCRL1 $-/-$ (Fig. 3B, top). The specificity of blotting was confirmed by injecting an ATG-blocking morpholino (MO) into wild-type (WT) embryos, which also significantly reduced OCRL1 protein levels (Fig. 3B, bottom). Previous analysis of Lowe syndrome patients' cells revealed an increase in PtdIns(4,5)$P_2$ levels by 1.9–2.1-fold when compared with controls, consistent with the loss of OCRL1 5-phosphatase activity in Lowe syndrome (39,40). We therefore wanted to determine whether the OCRL1 mutant embryos displayed elevated levels of PtdIns(4,5)$P_2$. For this purpose, we developed a metabolic labelling protocol allowing the measurement of phosphoinositide lipids in zebrafish embryos at 48 hpf. Using this method, we could show that OCRL1 mutant embryos have a 1.8-fold increase in PtdIns(4,5)$P_2$, comparable with that seen in Lowe syndrome patients (Fig. 3C).

## OCRL1-deficient embryos have increased susceptibility to seizures

Lowe syndrome patients are prone to generalized motor seizures, and are nine times more likely to experience febrile convulsions compared with healthy subjects (2,34). We therefore investigated whether the OCRL1-deficient mutant embryos display a similar susceptibility to heat-induced seizures. Electrophysiological recordings taken from the forebrain of OCRL1 mutant and control embryos revealed that while the temperature for seizure initiation is the same for control and mutant embryos, the OCRL1 mutants have significantly longer seizure duration than the control (Fig. 4A, C and D). The increased activity in the mutants can also be seen in a power analysis of seizure amplitude versus frequency (Fig. 4B). We failed to observe spontaneous seizure activity over the 45 min duration of the electrophysiological recordings. However, casual inspection of freely behaving juvenile and adult mutants indicates that they occasionally undergo uncontrolled twitching followed by rigor before recovering,

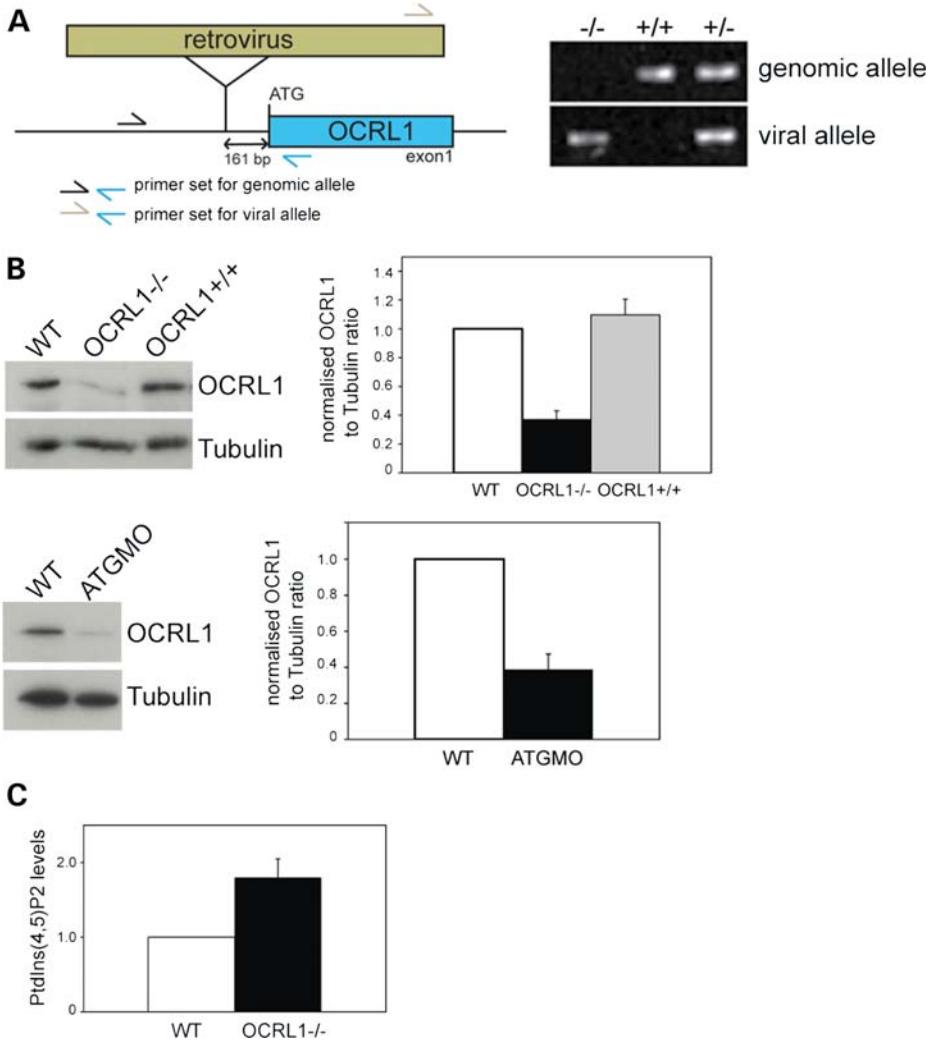


**Figure 3.** A zebrafish mutant deficient in OCRL1 has elevated PtdIns(4,5)$P_2$ levels. (**A**) Left: Schematic diagram showing the location of the retroviral insertion upstream of the OCRL1 start codon. Primers used to amplify genomic DNA from zebrafish embryos are indicated. Right: Agarose gel analysis of DNA amplified from OCRL1−/−, +/− and +/+ embryos using the indicated primer pairs. (**B**) Western blotting of WT, OCRL1−/− and OCRL1+/+ zebrafish embryos at 2 dpf, or embryos injected with a translation-blocking OCRL1 morpholino (ATGMO). Representative blots and quantitation are shown. Results are expressed as the mean + SEM from five experiments. (**C**) Quantitation of PtdIns(4,5)$P_2$ levels in WT and OCRL1−/− embryos at 2 dpf. Results are expressed as the mean + SEM from six experiments.

suggesting that they may be prone to spontaneous seizures during their lifetime.

## OCRL1-deficient zebrafish have reduced survival and growth

Ocular and neurological symptoms of Lowe syndrome are present at birth, indicating early developmental defects in humans (2). The increased susceptibility of OCRL1 mutant embryos to seizures indicates the early appearance of neurological abnormalities in this model. We therefore assessed viability of the OCRL1 mutant zebrafish. Strikingly, we observed a 60% mortality rate for the mutant in the first 3 weeks of life, compared with only 20% for the WT controls (Supplementary Material, Fig. S3). This 3-fold increase in mortality is consistent with the developmental defects attributable to OCRL deficiency leading to reduced viability. Lowe syndrome is characterized by growth retardation in the early years of life. We therefore analysed growth in the OCRL1 mutants. As shown in Supplementary Material, Fig. S4, juvenile OCRL1 mutant zebrafish are reduced in length when compared with WT controls at both 1 and 2 months. This is consistent with a growth defect similar to that seen in human patients.

## Cystic brain lesions are present in OCRL1-deficient zebrafish

Brain abnormalities have been reported in MRI images of Lowe syndrome patients (2,34–36). These typically correspond to periventricular cysts and white matter changes consistent with gliosis. We therefore performed micro-MRI (μMRI) imaging to determine whether similar changes would be present in the

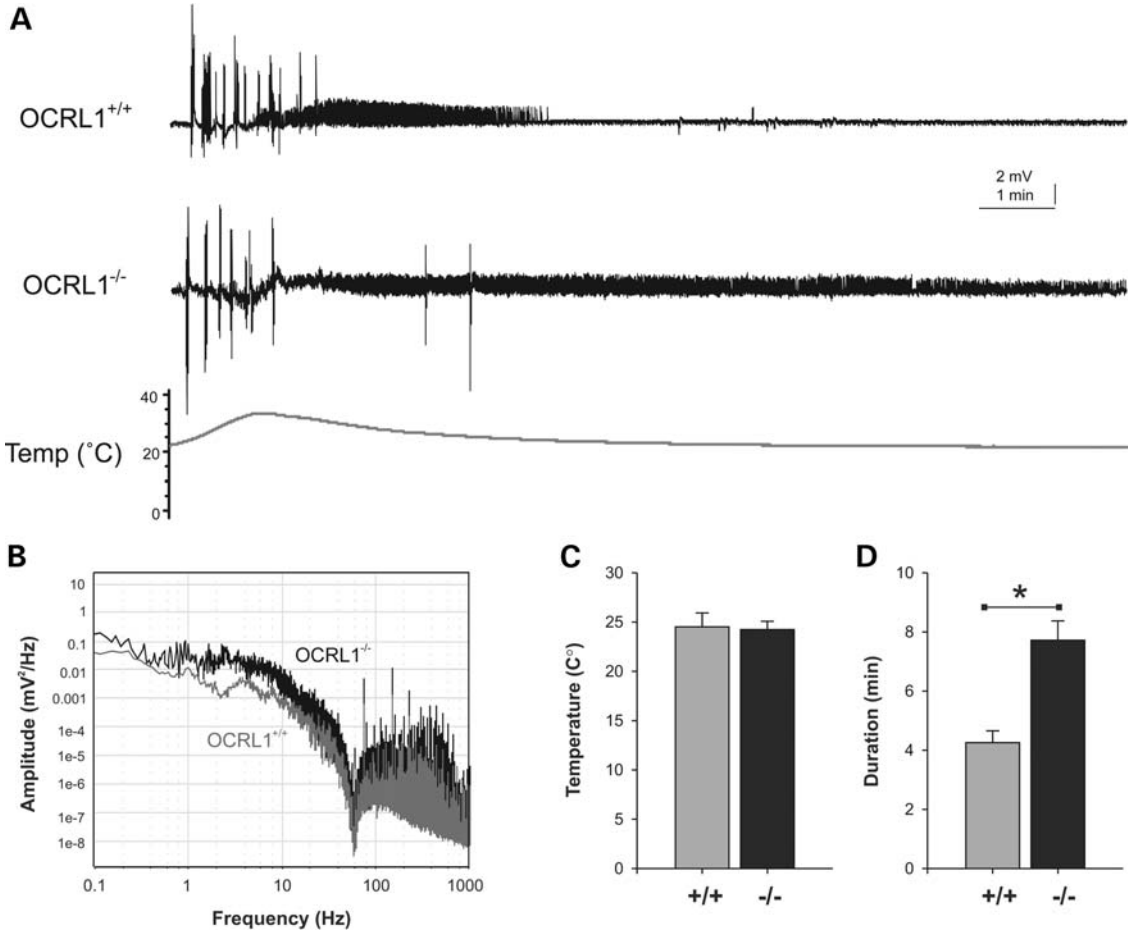


**Figure 4.** Electrographic seizure activity in OCRL1 mutant zebrafish. (**A**) Representative recoding taken from the forebrain of parental OCRL1$^{+/+}$ and OCRL1$^{-/-}$ mutant zebrafish embryos at 6 dpf. (**B**) Plot of amplitude versus frequency of recordings taken from OCRL1$^{+/+}$ and OCRL1$^{-/-}$ embryos. (**C**,**D**) Plot of average temperature at onset of seizure (C) and duration of seizure activity (D) in OCRL1$^{+/+}$ and OCRL1$^{-/-}$ embryos. Data are presented as mean + SEM ($n = 23-30$). *$P < 0.001$.

OCRL1 mutant zebrafish. We used adult animals for this analysis as embryos and juveniles are not amenable to MRI. We could detect white matter lesions in all eight mutant fish analysed, while none were detected in eight WT controls (Fig. 5A, left). The lesions were always in the periventricular region, and appeared to be filled with cerebrospinal fluid according to MRI T2 relaxation times (Supplementary Material, Fig. S5). The nature of the lesions was further investigated using immunohistochemistry. We observed strong glial fibrillary acid protein (GFAP) staining in the lesions when compared with elsewhere in the brain, consistent with increased numbers of astrocytes in these regions, indicative of gliosis (Fig. 5B, right). In contrast, GFAP staining was largely absent from the periventricular region of control animals. OCRL1-deficient zebrafish therefore develop white matter abnormalities similar to those reported in Lowe syndrome patients.

### OCRL1 deficiency impairs neural development during embryogenesis

The presence of neurological abnormalities, namely increased seizure susceptibility, in OCRL1-deficient zebrafish embryos suggests that OCRL1 may play a role in neural development during embryogenesis. We therefore analysed the OCRL1-deficient mutant embryos in more detail. The morphology of mutant embryos was assessed at different stages of development. The most striking phenotype is the reduction in the size of the brain and eyes of OCRL1 mutant embryos, which is most obvious at 1 dpf (Fig. 6A). The reduced size of these tissues does not simply reflect smaller overall size of the mutant embryos, as this was the same as WT embryos at 1 dpf (data not shown). The midbrain–hindbrain boundary is less defined when compared with controls at this stage, and the eyes are underdeveloped. There are however no obvious cataracts or opacities in the lens of mutant embryos. The mutant embryos also have a reduction in pigmentation that is also seen at later stages (Supplementary Material, Fig. S4A and data not shown). To better assess the reduction in brain size in the mutants, we performed confocal microscopy of the head region of whole-mount embryos, and histology on transverse sections taken through different regions of the head. Both approaches revealed a significant reduction in neural tissue in the fore-, mid- and hindbrain regions of mutants at 1 dpf (Fig. 6B and C). Importantly,

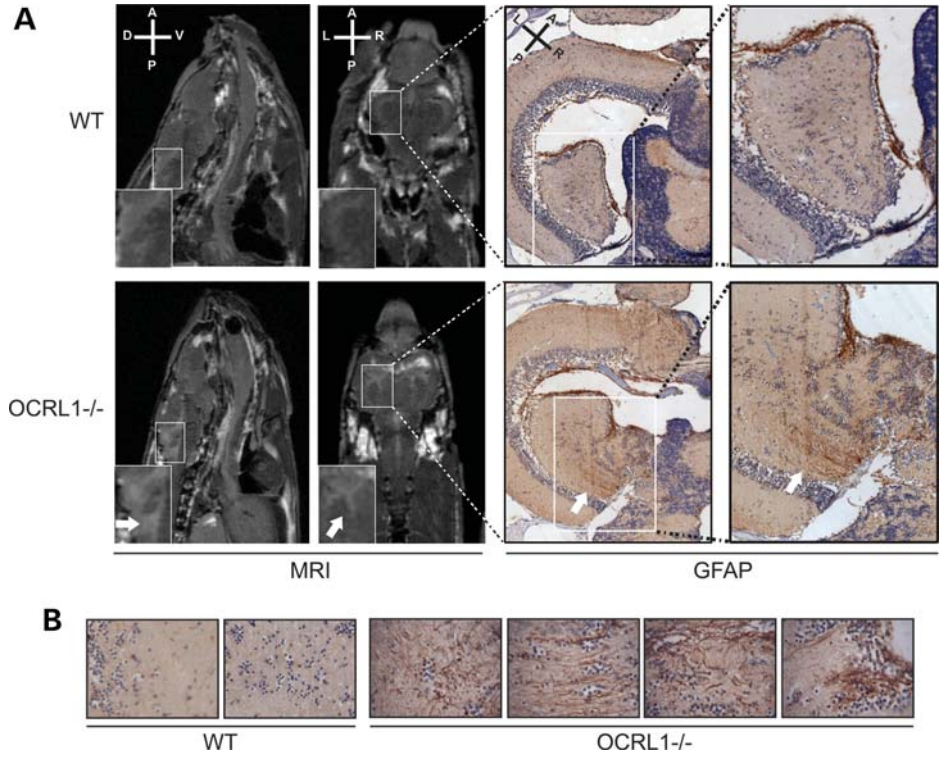


**Figure 5.** White matter lesions in OCRL1 mutant zebrafish. (**A**) Transverse relaxation (T2)-weighted MRI images of the brains of WT and OCRL1−/− adult zebrafish. Sagittal images indicate the presence of a white matter anomaly (white arrow in insert) in OCRL−/−, which was not seen in WT. Coronal images show the presence of lesions adjacent to the ventricles (white arrow in insert). Immunohistochemistry was carried out on the same samples used for MRI. A higher number of GFAP-positive astrocytes are present in the periventricular lesion suggesting increased gliosis. (**B**) Examples of GFAP staining of WT and OCRL1−/− brain regions. Note the increased numbers of astrocytes concentrated in regions that correspond to periventricular lesions of OCRL1−/− embryos.

these differences are not due to a general developmental delay. Embryos were confirmed to be at the same stage of development according to somite number (Supplementary Material, Fig. S7). Moreover, time-lapse microscopy showed that the OCRL1-deficient embryos progress through the first 18 h of embryogenesis at the same rate as controls, as assessed by gross morphology, arguing against a general developmental delay in the mutants (Supplementary Material, Fig. S6 and Movie S1).

The morphological changes described above are specific to loss of OCRL1. Firstly, they are phenocopied by injection of an ATG MO that efficiently knocks down OCRL1 expression (Figs 3B and 6A). For the MO injections, we used p53-deficient embryos to minimize off-target effects (41). Secondly, the morphological differences seen in both the mutant and morphant embryos are rescued, at least partially, by re-expression of WT GFP-tagged zebrafish OCRL1 (Fig. 6D). We do not observe changes in the patterning or levels of expression of various markers of brain region specification analysed at 1 dpf, including *foxG1* (telenecephalon), *otx3* (midbrain), *hoxb1a* (rhombomere 4) and *hoxb4* (rhombomeres 6 and 7) (Supplementary Material, Fig. S7). With *pax2.1* (optic stalk, MHB and otic vesicle), we observed a reduction in length between the optic stalk, MHB and otic vesicle, consistent with a reduction in brain size at this point in development (Supplementary Material, Fig. S7). Similarly, *krox20* labelling displays a similar pattern between mutant and control embryos, but with reduced separation between rhombomeres 3 and 5 in the mutant consistent with a reduced brain size.

## OCRL1 is required for Akt signalling and cell survival and proliferation during embryogenesis

The impaired development of the brain in OCRL1 mutant and morphant embryos is consistent with the high level of OCRL1 expression in this tissue. OCRL1 has previously been implicated in several cellular processes including membrane traffic and intracellular signalling, both of which are important for neural development. To determine whether deficiency of OCRL1 affects intracellular signalling during embryogenesis, we determined the activation status of two major signalling pathways, namely the MAPK and Akt pathways, using phospho-specific antibodies. There were comparable levels of phospho-ERK in mutant and WT embryos, indicating that MAPK signalling was unaffected by OCRL1 deficiency (Fig. 7A). In contrast, Akt signalling was noticeably attenuated in the OCRL1 mutant, indicated by a reduction in phospho-Akt reactivity. Interestingly, total Akt levels also appeared reduced in the OCRL1 mutants, suggesting a defect in signalling pathways upstream of Akt expression. The reduction in phospho- and total Akt levels were rescued by expression of GFP–OCRL1, indicating the specificity of these effects (Fig. 7A). The Akt pathway is most commonly associated with cell survival, so we decided to investigate whether apoptosis may be increased in the OCRL1 mutant beyond the naturally occurring level seen in embryogenesis. Using both acridine orange labelling of live embryos and TUNEL staining of fixed embryos, we found a significant

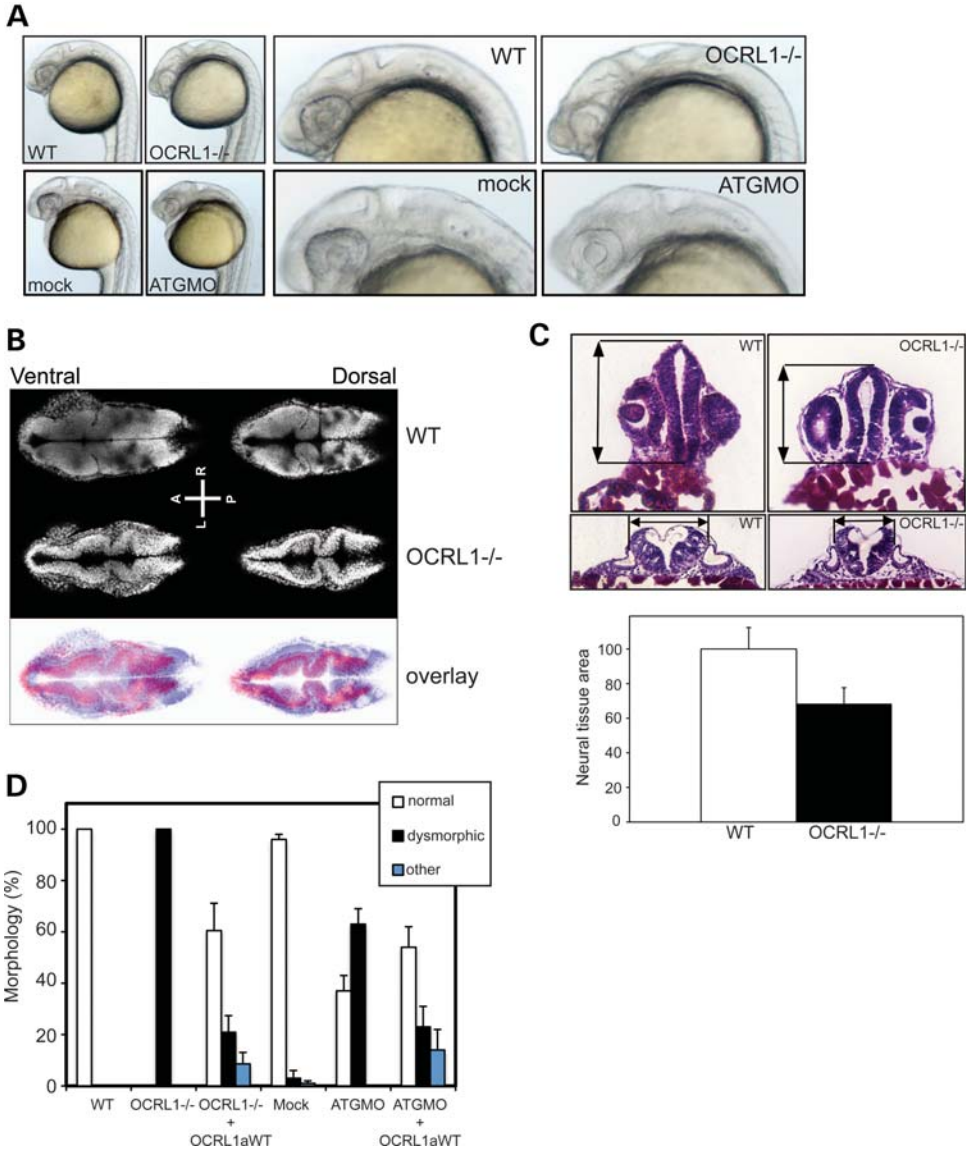


**Figure 6.** Impaired development of the brain and eyes in OCRL1-deficient embryos. (**A**) Representative bright field images of 26 hpf WT and OCRL1 −/− uninjected embryos, or WT embryos injected with either mock or ATGMO morpholino. (**B**) Confocal slices of 1 dpf WT and OCRL1 −/− embryos stained with DRAQ5 to label the nuclei. The overlay is false-coloured with WT staining in blue and OCRL1 −/− in red. (**C**) Representative H&E-stained cryosections from the forebrain (top) or R5 hindbrain region (bottom) of 1 dpf WT and OCRL1 −/− embryos. Arrows indicate the reduction in size of these regions in the OCRL mutant. Quantitation of neural tissue cross-sectional area of forebrain sections. Data are expressed as the mean + SEM ($n = 10$). (**D**) Quantitation of morphological phenotype. Results are expressed as the mean + SEM ($n = 63–501$ embryos from 4 to 13 experiments). The WT morphology is normal. Dysmorphic describes embryos with a smaller head and eyes and loss of defined MHB. This phenotype is seen in both OCRL1 morphant and mutant embryos. Other describes embryos with more severe anatomical defects not restricted to the brain and eyes that may arise from high-level over-expression of OCRL1a.

increase in apoptosis in the mutant embryos (Fig. 7B and Supplementary Material, Fig. S8). Apoptotic cells were present throughout the embryo, indicating a global defect in cell survival. Importantly, a comparable increase in apoptosis was observed in OCRL1 MO-injected p53-deficient embryos (Supplementary Material, Fig. S8). The increased apoptosis seen in both mutant and morphants could be rescued by re-expression of GFP-tagged OCRL1, indicating that these effects are specific to loss of OCRL1 (Fig. 7B).

Proliferation was also assessed in the OCRL1 mutant embryos using phospho-histone H3 (PH3) as a marker for mitotic cells. Proliferating cells were present throughout WT embryos but most evident in the periventricular region where the bulk of neurogenesis takes place (Fig 7C, arrows and Supplementary Material, Movie S2). In OCRL1 mutant embryos, there was a clear reduction in PH3 staining, indicating reduced levels of proliferation. The striking loss of PH3 staining in the periventricular region is consistent with impaired neurogenesis in the mutant. As observed for morphology, Akt activation and apoptosis, the reduced levels of proliferation observed in the mutant were rescued by re-expression of GFP-tagged OCRL1 (Fig. 7C). Together, these results indicate an important role for OCRL1 in Akt signalling, cell survival and proliferation during embryogenesis.

### OCRL1 catalytic activity and clathrin binding are essential for OCRL1 function *in vivo*

To determine the cellular mechanisms underlying the defects, we observe in OCRL1 mutant and morphant embryos, rescue experiments were performed using constructs with point mutations that abrogate catalytic activity (D480A) or binding to the vesicle coat protein clathrin (△LIDLE). Morphology, apoptosis and proliferation were scored to determine the ability of each construct to rescue these phenotypes. Importantly, expression levels of the various constructs were comparable as assessed by GFP fluorescence. Expression of the catalytically inactive D480A mutant failed to rescue mutant morphology, apoptosis or proliferation, indicating that 5-phosphatase activity is essential for OCRL1 function *in vivo* (Fig. 8A–C). Interestingly, expression of this construct led to a more severe morphological defect than that seen in the mutant alone, with a greater reduction in the size of the brain (Fig. 8A). Moreover, we observed enhanced apoptosis in embryos expressing the D480A mutant (Fig. 8B). This was particularly striking in the head, suggesting increased apoptosis within the neural tissue. We also observed a greater reduction in cell proliferation in mutant embryos expressing the D480A mutant (Fig. 8C). These results confirm the functional importance of OCRL1 5-phosphatase activity during embryonic development.

OCRL1 interacts with clathrin through two binding sites, LIDIA (LIDID in zebrafish) and LIDLE, which are found on flexible loops protruding from the PH and RhoGAP-like domains, respectively (8,15). We have previously shown that the second site is most important for localization of OCRL1 to clathrin trafficking intermediates in cells (15). Differential splicing of OCRL1 occurs next to this site, which alters its ability to interact with clathrin, such that splice isoform a binds better than isoform b, and as a result is more enriched in clathrin-coated trafficking intermediates (15). Isoform a is the only form of OCRL1 in brain, while in other tissues both forms are expressed, suggesting that clathrin binding is important for OCRL1 in the brain. To test this hypothesis in the context of embryonic development, and to gain a better mechanistic explanation for the phenotypes we observe, rescue experiments were performed using mutant OCRL1 lacking the LIDLE motif. As shown in Fig 8A, the △LIDLE construct was unable to rescue the mutant phenotype at the morphological level. In fact, in ∼30% of embryos, the reduction in brain size was more severe than in the mutant embryos alone. The △LIDLE mutant was also compromised in its ability to rescue the increased apoptosis and reduced proliferation seen in the mutant embryos (Figs 8B and C). To further assess the significance of clathrin binding and OCRL1 splicing, rescue experiments were performed with the b isoform of OCRL1. This construct failed to efficiently rescue the morphological, apoptosis and proliferation defects seen in the mutant, confirming the importance of clathrin binding (Fig. 8A–C). Together, our results indicate that 5-phosphatase activity and interaction with clathrin are important for OCRL1 function during embryonic brain development.

## DISCUSSION

In this study, we report for the first time, a zebrafish model for Lowe syndrome. This model recapitulates several of the neurological features of Lowe syndrome including increased susceptibility to heat-induced seizures and white matter lesions. Attempts to generate a mouse model for studying the neurological component of Lowe syndrome have so far failed, most likely due to compensation of OCRL1 by murine INPP5B (30), which is spliced differently in this organism to other vertebrates (42). Although zebrafish expresses INPP5B, it is unable to compensate for the loss of OCRL1 in the neurological tissue, as seen for human Lowe syndrome patients. Zebrafish OCRL1 and INPP5B are highly conserved with their human counterparts in terms of sequence identity and domain organization. Moreover, zebrafish OCRL1 has the same subcellular localization as the human protein, and is identical in its tissue-specific expression and splicing. Together, these observations indicate that zebrafish is a good model to investigate the disease mechanisms of Lowe syndrome. In further support of this assertion, we observe a 1.8-fold increase in PtdIns(4,5)$P_2$ levels in OCRL1-deficient zebrafish embryos, which is similar to the increase seen in cells derived from Lowe syndrome patients (39,40). Such an increase in PtdIns(4,5)$P_2$ levels indicates that despite the presence of numerous 5-phosphatase enzymes in vertebrates, OCRL1 contributes a significant proportion of total 5-phosphatase activity.

Several of the neurological defects in Lowe syndrome patients are evident at birth, suggesting a developmental role for OCRL1 within the central nervous system (1,2). Using the zebrafish model, we can now demonstrate that this is indeed the case. The most striking developmental defect is reduction in the size of the brain and eyes when observed at 1 dpf. This phenotype is specific: it is observed with both morphant and mutant embryos that are deficient in OCRL1, and it is rescued by re-expression of WT OCRL1. Importantly, the mutant/morphant phenotype is not due to a general developmental delay, as assessed by somite number and gross morphology. The morphological changes we observe therefore reflect a more specific defect in the development of the brain and eyes, tissues in which OCRL1 is particularly abundant. Defective neural development likely accounts for the impaired functionality of the brain that is observed in OCRL1 mutants, namely increased susceptibility to heat-induced seizures, which is evident already at 6 dpf. This mimics the situation in Lowe syndrome, where increased febrile seizures are seen in young and older patients alike (2,34). Whether seizures account for the 3-fold higher mortality of juvenile OCRL1 mutant embryos is hard to say, but it is interesting to note that epileptic seizures are a frequent cause of death in Lowe syndrome patients (2). Those mutant zebrafish that do survive through to adulthood have a brain size comparable with controls, as assessed by μMRI imaging. However, in all mutant embryos, we observed periventricular lesions in the brain, consistent with impaired functionality of this organ. These lesions may be a long-term consequence of defects occurring during development of the neural tissue, resulting in suboptimal organization of neuronal networks, which in the longer term causes increased cumulative neuronal death. Alternatively, neuronal death in adults may arise through defects intrinsic to the neurons themselves. This could occur through defective clathrin-mediated trafficking that is important not only for synaptic vesicle recycling but also receptor localization and responsiveness of post-synaptic

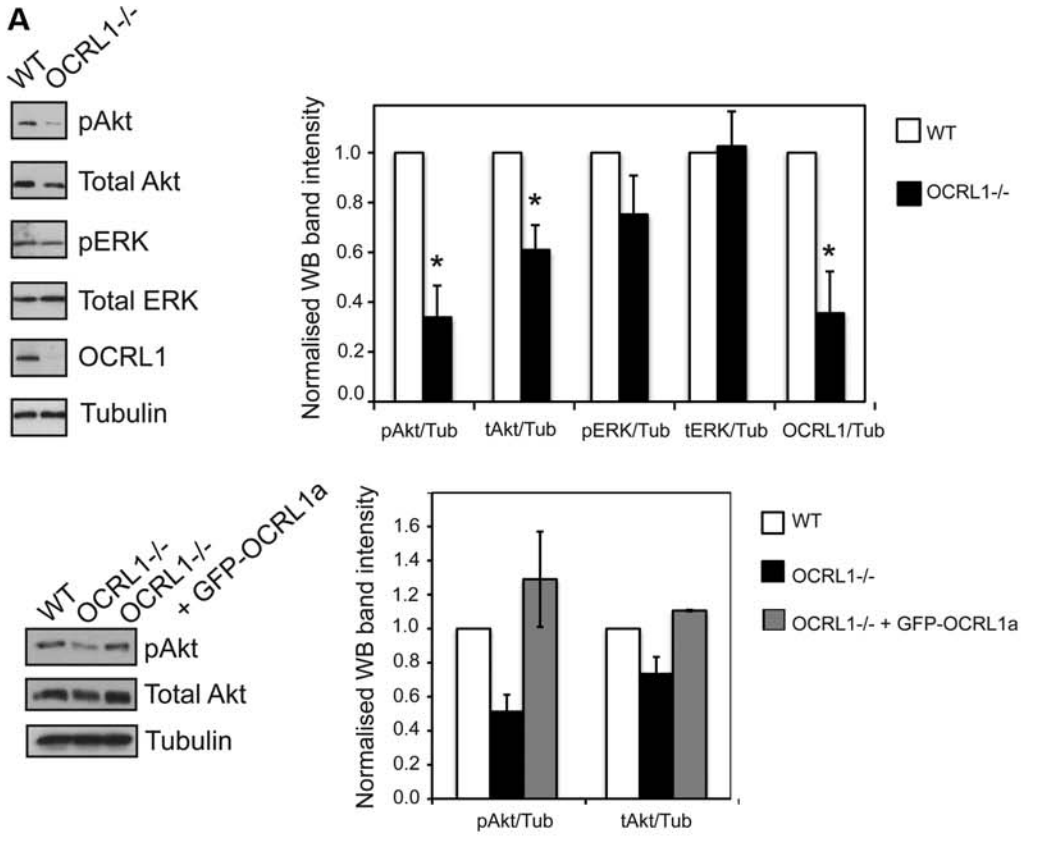
A
WT
OCRL1-/-
pAkt
Total Akt
pERK
Total ERK
OCRL1
Tubulin
Normalised WB band intensity
1.0
0.8
0.6
0.4
0.2
0.0
*
pAkt/Tub
tAkt/Tub
pERK/Tub
tERK/Tub
OCRL1/Tub
WT
OCRL1-/-
WT
OCRL1-/-
OCRL1-/-
+ GFP-OCRL1a
pAkt
Total Akt
Tubulin
Normalised WB band intensity
1.6
1.4
1.2
1.0
0.8
0.6
0.4
0.2
0.0
pAkt/Tub
tAkt/Tub
WT
OCRL1-/-
OCRL1-/- + GFP-OCRL1a

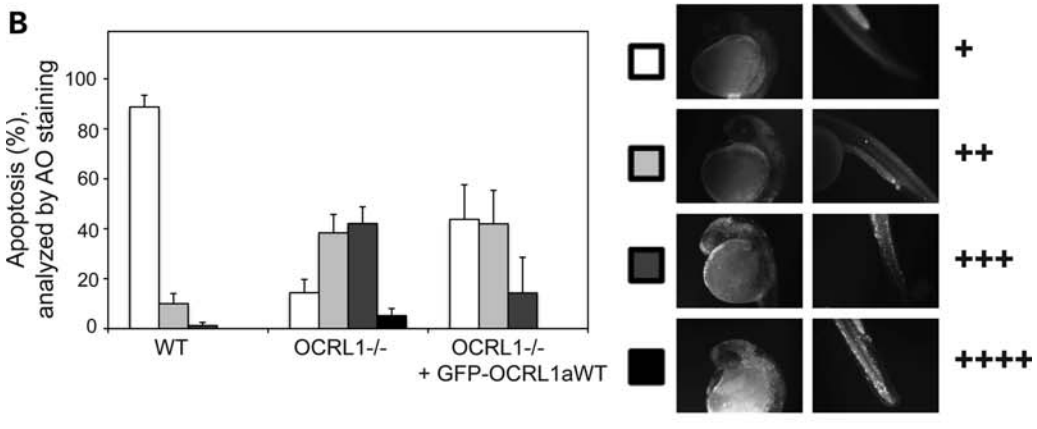
B
Apoptosis (%),
analyzed by AO staining
100
80
60
40
20
0
WT
OCRL1-/-
OCRL1-/-
+ GFP-OCRL1aWT
+
++
+++
++++

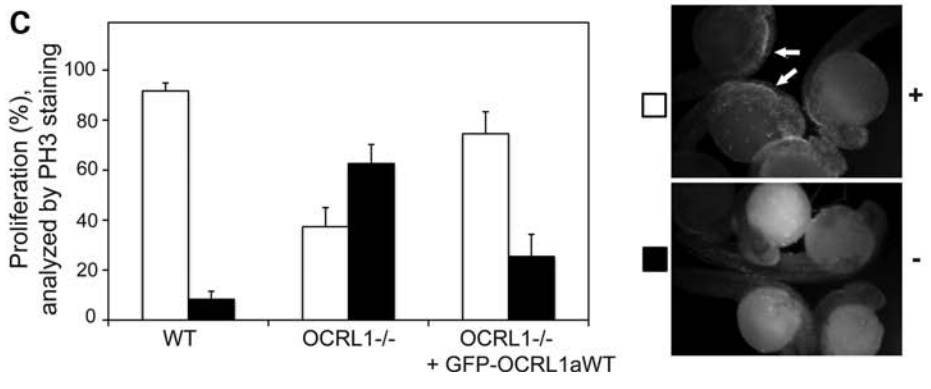
C
Proliferation (%),
analyzed by PH3 staining
100
80
60
40
20
0
WT
OCRL1-/-
OCRL1-/-
+ GFP-OCRL1aWT
+
-

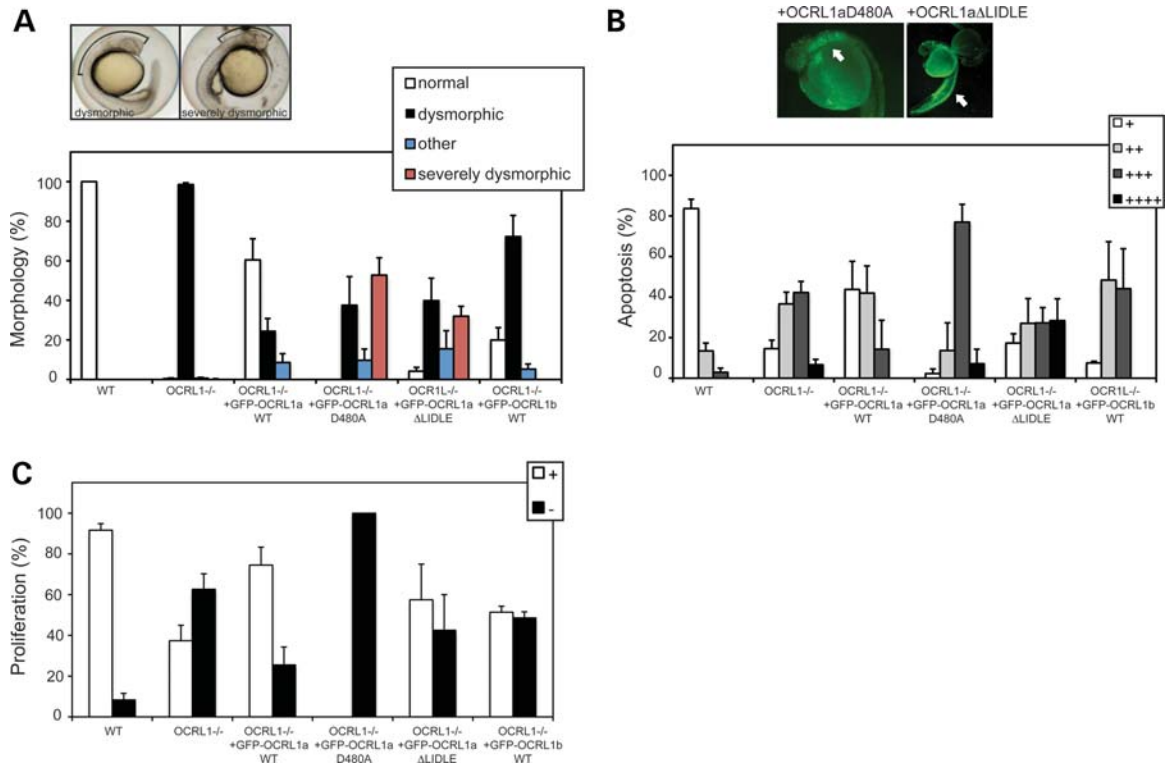


**Figure 8.** Catalytic activity and binding to clathrin are required for OCRL1 function in brain development. (**A**) Representative bright field images of 26 hpf OCRL1 −/− mutant embryos either uninjected (left) or injected with mRNA encoding GFP–OCRL1 D480A (right). The phenotypes were scored as dysmorphic (left) or severely dysmorphic (right), in which the brain size is further reduced when compared with the mutant alone. Quantitation of the morphological phenotypes obtained upon expression of the indicated constructs in OCRL1 −/− mutant embryos. Results are expressed as the mean + SEM ($n = 38–324$ embryos from 2 to 18 experiments). (**B**) Representative AO staining of apoptosis in OCRL1 −/− mutant embryos expressing GFP–OCRL1 D480A or GFP–OCRL1 ΔLIDLE. Note the increased apoptosis in the head region (left) and spinal cord (right), indicated by arrows. Quantitation of the AO staining obtained upon expression of the indicated constructs in OCRL1 −/− mutant embryos. Results are expressed as the mean + SEM ($n = 29–136$ embryos from 2 to 17 experiments). (**C**) Quantitation of proliferation as assessed by PH3 staining upon expression of the indicated constructs in OCRL1 −/− mutant embryos. Results are expressed as the mean + SEM ($n = 13–89$ embryos from 2 to 12 experiments).

cells. It has recently been shown that INPP4A, which hydrolyses PtdIns(3,4)$P_2$, is important for NMDA receptor localization and suppression of excitotoxic cell death (43). OCRL1, by regulating endocytic traffic, may also participate in this process.

We observe reduced Akt signalling and increased apoptosis in the OCRL1-deficient mutants. This indicates that OCRL1 is important for signalling through the Akt pathway. Conceivably, OCRL1 could directly regulate Akt through hydrolysis of PtdIns(3,4,5)$P_3$, which binds Akt to promote membrane recruitment and activation. It could also regulate Akt through altering levels of PtdIns(4,5)$P_2$, the precursor of PtdIns(3,4,5)$P_3$. However, we believe that these possibilities are unlikely as OCRL1 hydrolyses PtdIns(4,5)$P_2$ and PtdIns(3,4,5)$P_3$, and so any loss of activity would be expected to increase Akt activation, which is contrary to what we see. Another possibility is that OCRL1 regulates Akt through its association with the endosomal scaffolding protein APPL1, which is important for Akt signalling from endosomes. Indeed, MO-induced knockdown of APPL1 in zebrafish leads to increased apoptosis in the nervous system (44). However, proliferation is unaffected in APPL1 morphants, indicating that the mechanisms underlying the neurological defects we observe are not the same as those in APPL1

**Figure 7.** Decreased Akt signalling, cell survival and proliferation in OCRL1-deficient embryos. (**A**) Top: western blotting of 1–4 dpf WT and OCRL1 −/− embryo extracts with the indicated antibodies. Representative blots and quantitation are shown. Results are expressed as the mean + SEM from five experiments. $^*P < 0.01$. (A) Bottom: Extracts from 1 dpf WT, OCRL1 −/− embryos or OCRL1 −/− embryos expressing GFP–OCRL1 isoform a were analysed by western blotting with the indicated antibodies. Quantitation from two experiments is shown, with error bars indicating the range of values obtained. (**B**) WT, OCRL1 −/− and OCRL1 −/− embryos expressing GFP–OCRL1 isoform a at 28 hpf were labelled with acridine orange (AO) to label apoptotic cells. Embryos with different levels of apoptosis were divided into four categories as indicated: from + to ++++. Embryos in each category were counted and data are presented as the mean + SEM ($n = 37–96$ embryos from 3 to 12 experiments). (**C**) WT, OCRL1 −/− and OCRL1 −/− embryos expressing GFP–OCRL1 isoform a at 28 hpf were stained with anti-phosphohistone H3 (PH3) to label mitotic cells. Note the abundance of mitotic cells in the head region, where they align next to the ventricle boundary (arrows). Embryos were scored as having normal staining indicating WT levels of proliferation (+) or weak staining indicating clearly reduced proliferation (−). Embryos in each category were counted and data are presented as the mean + SEM ($n = 35–89$ embryos from 4 to 12 experiments).

morphants. APPL1 is recruited to endosomes independently of OCRL1, and the significance of OCRL1 binding for APPL1 function in signalling is so far unclear (7). We cannot exclude the possibility that OCRL1 participates in APPL1-mediated Akt signalling, but our data are more consistent with reduced Akt signalling arising from defects in membrane traffic. OCRL1 lacking the LIDLE clathrin-binding site, which is required for OCRL1 incorporation into clathrin-coated trafficking intermediates (15), fails to rescue apoptosis in the mutant. A similar result is seen with the isoform b of OCRL1, in which the LIDLE motif is inaccessible for clathrin-binding. This indicates that OCRL1 functions in the context of clathrin-mediated trafficking to promote Akt signalling.

Neurotrophin receptors, which play a key role in neuronal survival, differentiation and proliferation, are internalized in a clathrin-dependent manner and delivered to endosomes. Cell survival signalling requires retrograde trafficking of neurotrophin receptor-containing endosomes (45). Interestingly, it has recently been shown that regulated actin disassembly on endosomes is required to promote endosomal maturation and survival signalling (46). Loss of OCRL1 causes increased PtdIns(4,5)$P_2$ levels on endosomes, which results in the accumulation of actin and perturbation of endocytic trafficking (23). OCRL1 could therefore regulate Akt signalling in neurons by promoting endosomal actin disassembly to promote retrograde movement of neurotrophin receptor-containing endosomes. Of course, defective endocytic trafficking is likely to impact upon other signalling pathways active during neuronal development that may contribute to the phenotypes we observe upon depletion of OCRL1. Indeed, it has been demonstrated that OCRL1 regulates trafficking to the cilium, which is important for ciliogenesis (47). Defects in this pathway, which is independent of clathrin binding, are likely to contribute to defective signalling through primary cilia (47). Thus, OCRL1 is likely to regulate multiple trafficking routes that in turn influence several developmental signalling pathways. Our findings strongly suggest that a significant component of the neurological dysfunction seen in Lowe syndrome is due to defective clathrin-mediated trafficking of receptors.

Akt signalling is important for several cellular processes in addition to cell survival. Among these include proliferation and cell migration. The reduced Akt signalling in OCRL1-deficient embryos could therefore account for the reduction in proliferation we observe, as could perturbation of other signalling pathways. Another possibility is that defective cell division plays a role. OCRL1 was recently shown to participate in cytokinesis (10,25), suggesting that impairment of this process during embryogenesis could contribute to the phenotype we observe. This may be the case, but it should be noted that during the early stages of embryogenesis, e.g. up to and including gastrulation, we see no apparent defect in cell division *per se* in the OCRL1-deficient embryos (data not shown). Thus, the extent to which a cytokinesis defect contributes to Lowe syndrome pathology remains unclear. We also failed to observe defects in conversion and extension movements during gastrulation (data not shown), arguing against major defects in cell migration at this time. However, we cannot exclude the possibility that cell migration, and in particular migration of neurons, is affected at later stages in development.

In summary, we have developed a new animal model to investigate Lowe syndrome. This model recapitulates several of the neurological features of Lowe syndrome. It has also allowed us to identify a role for OCRL1 in maintaining Akt signalling and cell survival during embryogenesis. We have been able to demonstrate that OCRL1 function during development is dependent upon its 5-phosphatase activity and binding to the clathrin machinery. Together, our results support a role for OCRL1 in maintaining developmental signalling pathways downstream of clathrin-mediated membrane traffic. The zebrafish model should prove useful in further dissecting the disease mechanisms of Lowe syndrome, not just within the central nervous system but also in the other affected tissues.

## MATERIALS AND METHODS

### Antibodies

Polyclonal antibodies to zebrafish OCRL1 were raised in sheep using GST-tagged N-terminus (amino acids 1–303) and affinity purified using His-tagged N-terminus OCRL1 covalently coupled to CNBr beads. Other polyclonal antibodies were sheep anti-Golgi-84 (48), goat anti-EEA1 (Santa Cruz Biotechnology), mouse anti-clathrin X22 (Liz Smythe, University of Sheffield, UK), mouse anti tubulin TAT-1 (Keith Gull, University of Oxford, UK), mouse acetylated tubulin (Sigma T7451), rabbit anti-PH3 Ser10 (Upstate 06570), rabbit GFAP (DAKO Z0334), rabbit pAkt (pSer473, Cell Signalling 4060S), rabbit Total Akt (Cell Signalling 9272), mouse pERK (Cell Signalling 9106S), mouse Total ERK (Cell Signalling 4696). Fluorophore Alexa594, Alexa488, cy3 and cy5) and horseradish peroxidase-conjugated secondary antibodies were purchased from Molecular Probes, Tago Immunologicals or Invitrogen.

### Molecular biology

All constructs were made using standard molecular biology techniques. Full-length *D. rerio* OCRLb cDNA was obtained from the MRC Geneservice as IMAGE clone 2600692.

A two-step mutagenesis insertion of the sequence GGA GAGGATAGCTGCATGGAAAAG was performed to make *D. rerio* OCRLa. Full-length OCRL1 isoforms a and b were cloned into a modified pcGlobin vector for N-terminal tagging with GFP, expression in tissue culture cells and *in vitro* synthesis of mRNA. Point mutations were introduced by PCR using the site-directed mutagenesis Quickchange method (Stratagene). An N-terminal fragment of OCRL1 encoding amino acids 1–303 was cloned into pGEX 4T-1 vector for bacterial expression of protein and antibody production. Fragments of OCRL (1–608 bp and 1765–2392 bp) were cloned into pCR + BluntII-TOPO (Invitrogen) for generation of ISH probes. DIG probes were generated with the DIG RNA labelling kit (SP6/T7, Roche) according to the manufacturer's instructions. Primer sequences for all manipulations are available upon request. All constructs were verified by DNA sequencing using the ABI PRISM Big dye Terminator TM Kit version 2 (PE Applied Biosystems). Plasmid encoding

human mCherry-tagged non-neuronal CLC was kindly provided by Dr Stephen Royle (University of Liverpool, UK).

### Zebrafish strains and husbandry

Zebrafish were raised and maintained at the University of Manchester Biological Services Unit as described (49). OCRL+/− F2 families were obtained from Znomics Inc. Inbreeding generated F3 embryos for genotyping. Further inbreeding generated F4–F6 embryos for analysis. All animal procedures were subject to local ethical review and performed under a Home Office license.

### RNA isolation, RT–PCR and genomic DNA isolation for genotyping

Total RNA was isolated from zebrafish larvae using Trizol (Invitrogen) and reverse-transcribed with Superscript First Strand (Invitrogen) to produce cDNA. For direct visualization of amplification products, cDNA was amplified using standard PCR conditions and appropriate primer pairs. For genotyping, genomic DNA was isolated by a HotSHOT DNA extraction procedure. Briefly, a tail clip was deposited into 100 μl 50 mM NaOH and heated for 20 min at 95°C. After cooling to 4°C, 10 μl 1 M Tris pH 8.0 was added and clarified by centrifugation and stored at −20°C.

### *In situ* hybridization

Embryos were dechorionated by pronase (Roche) and fixed in 4% buffered paraformaldehyde (PFA/PBS) overnight at 4°C. They were then washed three times in PBS containing 0.1% Triton X-100 (PBST) prior to being dehydrated in methanol at −20°C for at least 30 min. Embryos were rehydrated in descending concentrations of methanol in PBST solution. Embryos were treated with 10 μg/ml protease K (Sigma) for 15 min. After rinsing twice in 2 mg/ml glycine/PBST, embryos were fixed in 4% PFA/PBS for 20 min. Embryos were washed five times for 5 min in PBST solution and then briefly washed in 50% PBST/50% hybridization buffer, before incubating them in hybridization buffer for 1 h at 65°C. Hybridization was performed at 65°C overnight in hybridization buffer: 50% formamide, 5x saline-sodium citrate buffer (SSC), 0.5 mg/ml Torula yeast RNA (Sigma), 50 μg/ml Heparin, 0.1% Tween20 and 9 mM citric acid monohydrate pH 6.0–6.5 containing the DIG probe. Embryos were washed three times for 5 min in 50% hybridization buffer/50% 2x SSC at 65°C and then washed in descending concentrations of SSC in 0.1% Tween-20 solution at 65°C. Embryos were washed in descending concentration of 0.2x SSC in PBST solution. Embryos were blocked for 1 h in 5% fetal calf serum (FCS) in 10 mg/ml bovine serum albumin (BSA)/PBST prior to incubating them with anti-DIG-AP antibody (Roche) in 2 mg/ml BSA/PBST at 4°C overnight. After washing eight times in PBST, embryos were equilibrated in staining buffer (100 mM NaCl, 100 mM Tris–HCl, pH 9.5, 50 mM $MgCl_2$, 0.1% Triton X-100). For colour reaction, nitro blue terazolium/5-bromo-4-chloro-3-indolyl phosphate was used in staining buffer. Whole embryos were imaged on a Leica MZ6 stereomicrocope after fixing in either PFA or methanol, mounted in glycerol or benzyl alcohol/benzyl benzoate (BBA). For cryosections, embryos were embedded in gelatin solution (15% fish skin gelatin, 15% sucrose) overnight and frozen on dry ice for 30 min. The sections were cut at 30 μm thickness using a Leica cryostat, placed on SuperFrost Plus slides and kept at −80°C for at least 1 h. Slides were removed from −80°C and dried for 1 h, washed for 2 min in acetone, rehydrated for 1 min in PBS and mounted using Mowiol. Sections were imaged using Nikon Eclipse 80i microscope and processed using Photoshop CS2.

### Cell culture and immunofluoresence microscopy

AB9 cells were grown at 28°C and 5% $CO_2$ in Dulbecco's modified Eagle medium supplemented with 15% FCS and Penicillin/Streptomycin. PAC2 cells were grown at 28°C in L-15 medium containing 15% FCS and Penicillin/Streptomycin. Transient transfections were performed using Fugene HD (Roche Biochemicals, Indianapolis, IN, USA) according to the manufacturer's instructions using 2 μg DNA, 5 μg Fugene HD in 100 μl OptiMEM. Immunofluorescence microscopy was performed according to Choudhury and co-workers (14). Images were analysed using an Olympus BX60 upright microscope equipped with a MicroMax cooled, slow-scan charge-coupled device camera (Roper Scientific, Sarasota, FL, USA) driven by Metaview software (University Imaging Corporation, Sunnyvale, CA, USA). Images were processed using Adobe Photoshop CS5.

### RNA expression and morpholino injections in zebrafish

Capped mRNA encoding GFP–OCRL1 constructs was transcribed using the T7 mMessage mMachine kit (Ambion) and approximately 1 nl of a 0.4–1.0 μg/μl stock was injected into one-cell stage mutant embryos using a PLI-90 Pico-Injector (Harvard Apparatus). MO-modified antisense oligonucleotides targeting OCRL (ATGMO: AATCCCAA ATGAAGGTTCCATCATG) as well as a standard control MO (CCTCTTACCTCAGTTACAATTTATA) were obtained from GeneTools and 4–6 ng was injected into one-cell stage embryos.

### Magnetic resonance imaging

Adult zebrafish at 1 year of age were euthanized and were fixed in 4% PFA/PBS for 2 days and subsequently embedded in Fomblin. Micro-MRI imaging was performed according to Haud *et al*. (50).

### Immunohistochemistry

Adult zebrafish previously fixed in 4% PFA/PBS and analysed by μMRI were embedded in paraffin and 5 μm sections cut. The primary antibody was mouse anti-GFAP (1:300), incubated overnight at 4°C. The secondary antibody used was Vectastain biotinylated horse anti-pan-Ig antibody. Following incubation with secondary antibody, the sections were incubated with the ABC kit (Vectorlabs) and stained with DAB (Vectorlabs) before mounting with Pertex. Images were collected using a Zeiss Axioplan microscope and captured

using an Axiocam MR camera and Axiovision software (Zeiss). Images were then processed and analysed using Axiovision software (Zeiss), Photoshop CS5 and ImageJ.

### Time-lapse microscopy

Zebrafish embryos were collected 20 min post fertilization and placed in wells made of 0.7% agarose in chorion water (Instant Ocean). The embryos were incubated at 28°C and imaged using a Nikon TE2000 PFS microscope and Cascade II EMCCD camera with a dedicated manufacturer's software. Embryos were imaged every 5 min for 24 h. The images were processed using ImageJ software.

### Protein extraction and western blotting

Embryos were dechorionated by pronase and deyolked in Ginzburg buffer with protease inhibitor cocktail as described in the zebrafish book (49). Embryos were either extracted in native or denaturing conditions. For native conditions, buffer containing 1 mM Hepes, pH 7.4, 1 mM ethylene diamminetetraacetic acid, 15 mM $NaCl_2$, 0.5% Triton X-100, Protease Inhibitor Cocktail III (Calbiochem) and 20 mM β-glycerophosphate was used. Homogenization was performed for 2 min on ice with an Ultra-Turrax T8 (Ika-Werke), followed by 5 min incubation on ice. Supernatants were clarified by centrifugation at 20 000 *g* for 5 min in a microfuge at 4°C. For denaturing conditions, embryos were homogenized in the 20 mM Hepes, pH 7.4, 0.1 M NaCl, 1 mM dithiothreitol (DTT) buffer containing 1% sodium dodecylsulphate (SDS) with an Ultra-Turrax for 2 min on ice, then boiled for 3 min and an equal volume of 20 mM Hepes, pH 7.4, 0.1 M NaCl, 1 mM DTT buffer containing 4% Triton X-100 was added and re-homogenized for another 2 min on ice. Extracts were clarified in a microfuge. Adult tissues were extracted and immediately snap-frozen in liquid nitrogen. Proteins were extracted using the native extraction protocol. Protein was determined using the bicinchoninic acid method (Pierce) according to manufacturer's instructions and snap-frozen and stored at −80°C. Samples were boiled with SDS sample buffer prior to sodium dodecylsulphate–polyacrylamide gel electrophoresis and western blotting.

### Apoptosis and proliferation analysis

Zebrafish embryos at 24 hpf were stained with 5 μg/ml of Acridine Orange (Sigma) in embryo water for 30 min, and then washed three times for 5 min in embryo water. After anaesthesia with Tricaine (Sigma), AO staining was visualized using a Zeiss stereo Lumar V12 fluorescent microscope fitted with filter set Lumar 38 and images were acquired using an AxioCam MRm camera and processed using AxioVision software version 4.8 (Image Associates). TUNEL was performed with ApopTag Red *in situ* Apoptosis Detection Kit (Chemicon) according to the manufacturer's instructions. To analyse proliferation, whole-mount immunofluorescence was performed with anti-phospho Histone H3 antibodies. Briefly, dechorionated embryos were fixed in 4% PFA/PBS at 4°C overnight. Embryos were washed three times in methanol, and were rehydrated in descending concentrations of methanol in PBST solution. Primary antibody was incubated overnight at 4°C in 10% FBS/PBST. After six washes of 20 min in PBST, embryos were incubated in fluorescently tagged secondary antibody overnight at 4°C. After three washes of 15 min, embryos were imaged using the Zeiss stereo Lumar V12 fluorescent microscope.

### Lipid analysis

Zebrafish embryos at 48 hpf (60–80 embryos per labelling) were labelled in 500 μl chorion water (Instant Ocean) containing 300 μCi/ml $^{32}$P-orthophosphate for 2 h at 28°C. Thereafter, the fish were pelleted and total lipids were extracted using 500 μl of methanol, 200 μl of 2.4 M hydrochloric acid and 250 μl of chloroform and a Bioruptor Sonicator set at maximum amplitude for 2.5 min at room temperature. Phase separation was achieved by the addition of 250 μl of chloroform and 250 μl of milliQ water. Fifty micrograms of Folsch-extracted cow brain lipids (Sigma) was added to all samples to aid recovery of phosphoinositides. After centrifugation (20 000*g*, 5 min at room temperature), the upper phase was removed and replaced with theoretical upper phase. The samples were mixed, centrifuged and the lower phase was recovered into a new Eppendorf tube. The samples were dried in a vacuum centrifugal concentrator and then applied to a thin layer chromatography (TLC) plate for development once in the solvent mixture: chloroform/methanol/water/25% ammonia solution (45/35/8/2 v/v/v/v). After drying, radioactivity within the PtdIns(4,5)$P_2$ spot on the TLC plate was detected by phosphorimaging (PharosFX Plus with ImageOne software, BioRad). Confirmation that the spot on the TLC plate was PtdIns(4,5)$P_2$ was addressed by high-performance liquid chromatography (HPLC) analysis in parallel samples. Total lipids were first deacylated prior to HPLC analysis according to Jones *et al*. (51).

### Seizure analysis

Electrophysiological recordings of 6–7 dpf embryos were made from the forebrain according to Baraban *et al*. (52).

## SUPPLEMENTARY MATERIAL

Supplementary Material is available at *HMG* online.

## ACKNOWLEDGEMENTS

We would like to thank our colleagues for generously providing reagents as noted above. We are especially grateful to Dr Thomas Willnow (University of Berlin, Germany) for invaluable support at the beginning of the project, and to Professor Nancy Papalopulu (University of Manchester, UK) for discussions, advice and critically reading the manuscript. We would also like to thank Drs Karel Doray, Raphael Thuret, Alex Goonesinghe and Noemie Haud (University of Manchester, UK) for advice and discussion. We are grateful to Professor Jon Clarke (King's College, London) for generous help in teaching zebrafish microscopy techniques. We thank Peter March, Jane Knott and Robert Fernandez of the FLS

Bioimaging Facility for their help with microscopy. We are especially grateful to staff of the University of Manchester Biological Services Unit for animal caretaking and Miss Guanhua Yan for providing excellent technical support. Louise Stephen is thanked for her help in the early stages of the project. We also thank Professors Philip Woodman and Stephen High and Dr Shane Herbert for comments on the manuscript.

*Conflict of Interest statement*. None declared.

## FUNDING

This work was funded by a Wellcome Trust project grant (079615) and a research grant from the UK Lowe Syndrome Trust (ML/MU/DEC07) awarded to M.L. A.H. was supported by a Cancer Research UK Career Development Fellowship. Funding to pay the Open Access publication charges for this article was provided by the Wellcome Trust.

## REFERENCES

1. Lowe, C.U., Terrey, M. and Mac, L.E. (1952) Organic-aciduria, decreased renal ammonia production, hydrophthalmos, and mental retardation; a clinical entity. *Am. J. Dis. Child*, **83**, 164–184.
2. Loi, M. (2006) Lowe syndrome. *Orphanet J. Rare Dis.*, **1**, 16.
3. Attree, O., Olivos, I.M., Okabe, I., Bailey, L.C., Nelson, D.L., Lewis, R.A., McInnes, R.R. and Nussbaum, R.L. (1992) The Lowe's oculocerebrorenal syndrome gene encodes a protein highly homologous to inositol polyphosphate-5-phosphatase. *Nature*, **358**, 239–242.
4. Lowe, M. (2005) Structure and function of the Lowe syndrome protein OCRL1. *Traffic*, **6**, 711–719.
5. Hoopes, R.R. Jr., Shrimpton, A.E., Knohl, S.J., Hueber, P., Hoppe, B., Matyus, J., Simckes, A., Tasic, V., Toenshoff, B., Suchy, S.F. *et al.* (2005) Dent disease with mutations in OCRL1. *Am. J. Hum. Genet.*, **76**, 260–267.
6. Devuyst, O. and Thakker, R.V. (2010) Dent's disease. *Orphanet J. Rare Dis.*, **5**, 28.
7. Erdmann, K.S., Mao, Y., McCrea, H.J., Zoncu, R., Lee, S., Paradise, S., Modregger, J., Biemesderfer, D., Toomre, D. and De Camilli, P. (2007) A role of the Lowe syndrome protein OCRL in early steps of the endocytic pathway. *Dev. Cell*, **13**, 377–390.
8. Mao, Y., Balkin, D.M., Zoncu, R., Erdmann, K.S., Tomasini, L., Hu, F., Jin, M.M., Hodsdon, M.E. and De Camilli, P. (2009) A PH domain within OCRL bridges clathrin-mediated membrane trafficking to phosphoinositide metabolism. *EMBO J.*, **28**, 1831–1842.
9. Grieve, A.G., Daniels, R.D., Sanchez-Heras, E., Hayes, M.J., Moss, S.E., Matter, K., Lowe, M. and Levine, T.P. (2011) Lowe syndrome protein OCRL1 supports maturation of polarized epithelial cells. *PLoS One*, **6**, e24044.
10. Dambournet, D., Machicoane, M., Chesneau, L., Sachse, M., Rocancourt, M., El Marjou, A., Formstecher, E., Salomon, R., Goud, B. and Echard, A. (2011) Rab35 GTPase and OCRL phosphatase remodel lipids and F-actin for successful cytokinesis. *Nat. Cell Biol.*, **13**, 981–988.
11. Fukuda, M., Kanno, E., Ishibashi, K. and Itoh, T. (2008) Large scale screening for novel rab effectors reveals unexpected broad Rab binding specificity. *Mol. Cell Proteom.*, **7**, 1031–1042.
12. Hyvola, N., Diao, A., McKenzie, E., Skippen, A., Cockcroft, S. and Lowe, M. (2006) Membrane targeting and activation of the Lowe syndrome protein OCRL1 by rab GTPases. *EMBO J.*, **25**, 3750–3761.
13. Ungewickell, A., Ward, M.E., Ungewickell, E. and Majerus, P.W. (2004) The inositol polyphosphate 5-phosphatase Ocrl associates with endosomes that are partially coated with clathrin. *Proc. Natl Acad. Sci. USA*, **101**, 13501–13506.
14. Choudhury, R., Diao, A., Zhang, F., Eisenberg, E., Saint-Pol, A., Williams, C., Konstantakopoulos, A., Lucocq, J., Johannes, L., Rabouille, C. *et al.* (2005) Lowe syndrome protein OCRL1 interacts with clathrin and regulates protein trafficking between endosomes and the trans-Golgi network. *Mol. Biol. Cell*, **16**, 3467–3479.
15. Choudhury, R., Noakes, C.J., McKenzie, E., Kox, C. and Lowe, M. (2009) Differential clathrin binding and subcellular localization of OCRL1 splice isoforms. *J. Biol. Chem.*, **284**, 9965–9973.
16. Faucherre, A., Desbois, P., Nagano, F., Satre, V., Lunardi, J., Gacon, G. and Dorseuil, O. (2005) Lowe syndrome protein Ocrl1 is translocated to membrane ruffles upon Rac GTPase activation: a new perspective on Lowe syndrome pathophysiology. *Hum. Mol. Genet.*, **14**, 1441–1448.
17. Faucherre, A., Desbois, P., Satre, V., Lunardi, J., Dorseuil, O. and Gacon, G. (2003) Lowe syndrome protein OCRL1 interacts with Rac GTPase in the trans-Golgi network. *Hum. Mol. Genet.*, **12**, 2449–2456.
18. Lichter-Konecki, U., Farber, L.W., Cronin, J.S., Suchy, S.F. and Nussbaum, R.L. (2006) The effect of missense mutations in the RhoGAP-homology domain on ocrl1 function. *Mol. Genet. Metab.*, **89**, 121–128.
19. McCrea, H.J., Paradise, S., Tomasini, L., Addis, M., Melis, M.A., De Matteis, M.A. and De Camilli, P. (2008) All known patient mutations in the ASH-RhoGAP domains of OCRL affect targeting and APPL1 binding. *Biochem. Biophys. Res. Commun.*, **369**, 493–499.
20. Noakes, C.J., Lee, G. and Lowe, M. (2011) The PH domain proteins IPIP27A and B link OCRL1 to receptor recycling in the endocytic pathway. *Mol. Biol. Cell*, **22**, 606–623.
21. Swan, L.E., Tomasini, L., Pirruccello, M., Lunardi, J. and De Camilli, P. (2010) Two closely related endocytic proteins that share a common OCRL-binding motif with APPL1. *Proc. Natl Acad. Sci. USA*, **107**, 3511–3516.
22. Cui, S., Guerriero, C.J., Szalinski, C.M., Kinlough, C.L., Hughey, R.P. and Weisz, O.A. (2010) OCRL1 function in renal epithelial membrane traffic. *Am. J. Physiol. Renal Physiol*, **298**, F335–345.
23. Vicinanza, M., Di Campli, A., Polishchuk, E., Santoro, M., Di Tullio, G., Godi, A., Levtchenko, E., De Leo, M.G., Polishchuk, R., Sandoval, L. *et al.* (2011) OCRL controls trafficking through early endosomes via PtdIns4,5P2-dependent regulation of endosomal actin. *EMBO J.*, **30**, 4970–4985.
24. Coon, B.G., Mukherjee, D., Hanna, C.B., Riese, D.J. II, Lowe, M. and Aguilar, R.C. (2009) Lowe syndrome patient fibroblasts display Ocrl1-specific cell migration defects that cannot be rescued by the homologous Inpp5b phosphatase. *Hum. Mol. Genet.*, **18**, 4478–4491.
25. Ben El Kadhi, K., Roubinet, C., Solinet, S., Emery, G. and Carreno, S. (2011) The inositol 5-phosphatase dOCRL controls PI(4,5)P2 homeostasis and is necessary for cytokinesis. *Curr. Biol.*, **21**, 1074–1079.
26. Mitchell, C.A., Connolly, T.M. and Majerus, P.W. (1989) Identification and isolation of a 75-kDa inositol polyphosphate-5-phosphatase from human platelets. *J. Biol. Chem.*, **264**, 8873–8877.
27. Jefferson, A.B. and Majerus, P.W. (1995) Properties of type II inositol polyphosphate 5-phosphatase. *J. Biol. Chem.*, **270**, 9370–9377.
28. Schmid, A.C., Wise, H.M., Mitchell, C.A., Nussbaum, R. and Woscholski, R. (2004) Type II phosphoinositide 5-phosphatases have unique sensitivities towards fatty acid composition and head group phosphorylation. *FEBS Lett.*, **576**, 9–13.
29. Williams, C., Choudhury, R., McKenzie, E. and Lowe, M. (2007) Targeting of the type II inositol polyphosphate 5-phosphatase INPP5B to the early secretory pathway. *J. Cell Sci.*, **120**, 3941–3951.
30. Janne, P.A., Suchy, S.F., Bernard, D., MacDonald, M., Crawley, J., Grinberg, A., Wynshaw-Boris, A., Westphal, H. and Nussbaum, R.L. (1998) Functional overlap between murine Inpp5b and Ocrl1 may explain why deficiency of the murine ortholog for OCRL1 does not cause Lowe syndrome in mice. *J. Clin. Invest.*, **101**, 2042–2053.
31. Hellsten, E., Evans, J.P., Bernard, D.J., Janne, P.A. and Nussbaum, R.L. (2001) Disrupted sperm function and fertilin beta processing in mice deficient in the inositol polyphosphate 5-phosphatase Inpp5b. *Dev. Biol.*, **240**, 641–653.
32. Bothwell, S.P., Chan, E., Bernardini, I.M., Kuo, Y.M., Gahl, W.A. and Nussbaum, R.L. (2011) Mouse model for Lowe syndrome/Dent Disease 2 renal tubulopathy. *J. Am. Soc. Nephrol.*, **22**, 443–448.
33. Norden, A.G., Lapsley, M., Igarashi, T., Kelleher, C.L., Lee, P.J., Matsuyama, T., Scheinman, S.J., Shiraga, H., Sundin, D.P., Thakker, R.V. *et al.* (2002) Urinary megalin deficiency implicates abnormal tubular endocytic function in Fanconi syndrome. *J. Am. Soc. Nephrol.*, **13**, 125–133.
34. Erdogan, F., Ismailogullari, S., Soyuer, I., Ferahbas, A. and Poyrazoglu, H. (2007) Different seizure types and skin lesions in oculocerebrorenal syndrome of Lowe. *J. Child Neurol.*, **22**, 427–431.

35. Carvalho-Neto, A., Ono, S.E., Cardoso Gde, M., Santos, M.L. and Celidonio, I. (2009) Oculocerebrorenal syndrome of Lowe: magnetic resonance imaging findings in the first six years of life. *Arq. Neuropsiquiatr.*, **67**, 305–307.
36. Yuksel, A., Karaca, E. and Albayram, M.S. (2009) Magnetic resonance imaging, magnetic resonance spectroscopy, and facial dysmorphism in a case of Lowe syndrome with novel OCRL1 gene mutation. *J. Child Neurol.*, **24**, 93–96.
37. Nussbaum, R.L., Orrison, B.M., Janne, P.A., Charnas, L. and Chinault, A.C. (1997) Physical mapping and genomic structure of the Lowe syndrome gene OCRL1. *Hum. Genet.*, **99**, 145–150.
38. Johnson, J.M., Castle, J., Garrett-Engele, P., Kan, Z., Loerch, P.M., Armour, C.D., Santos, R., Schadt, E.E., Stoughton, R. and Shoemaker, D.D. (2003) Genome-wide survey of human alternative pre-mRNA splicing with exon junction microarrays. *Science*, **302**, 2141–2144.
39. Zhang, X., Hartz, P.A., Philip, E., Racusen, L.C. and Majerus, P.W. (1998) Cell lines from kidney proximal tubules of a patient with Lowe syndrome lack OCRL inositol polyphosphate 5-phosphatase and accumulate phosphatidylinositol 4,5-bisphosphate. *J. Biol. Chem.*, **273**, 1574–1582.
40. Wenk, M.R., Lucast, L., Di Paolo, G., Romanelli, A.J., Suchy, S.F., Nussbaum, R.L., Cline, G.W., Shulman, G.I., McMurray, W. and De Camilli, P. (2003) Phosphoinositide profiling in complex lipid mixtures using electrospray ionization mass spectrometry. *Nat. Biotechnol.*, **21**, 813–817.
41. Robu, M.E., Larson, J.D., Nasevicius, A., Beiraghi, S., Brenner, C., Farber, S.A. and Ekker, S.C. (2007) p53 activation by knockdown technologies. *PLoS Genet.*, **3**, e78.
42. Bothwell, S.P., Farber, L.W., Hoagland, A. and Nussbaum, R.L. (2010) Species-specific difference in expression and splice-site choice in Inpp5b, an inositol polyphosphate 5-phosphatase paralogous to the enzyme deficient in Lowe Syndrome. *Mamm. Genome*, **21**, 458–466.
43. Sasaki, J., Kofuji, S., Itoh, R., Momiyama, T., Takayama, K., Murakami, H., Chida, S., Tsuya, Y., Takasuga, S., Eguchi, S. *et al.* (2010) The PtdIns(3,4)P(2) phosphatase INPP4A is a suppressor of excitotoxic neuronal death. *Nature*, **465**, 497–501.
44. Schenck, A., Goto-Silva, L., Collinet, C., Rhinn, M., Giner, A., Habermann, B., Brand, M. and Zerial, M. (2008) The endosomal protein Appl1 mediates Akt substrate specificity and cell survival in vertebrate development. *Cell*, **133**, 486–497.
45. Ginty, D.D. and Segal, R.A. (2002) Retrograde neurotrophin signaling: Trk-ing along the axon. *Curr. Opin. Neurobiol.*, **12**, 268–274.
46. Harrington, A.W., St Hillaire, C., Zweifel, L.S., Glebova, N.O., Philippidou, P., Halegoua, S. and Ginty, D.D. (2011) Recruitment of actin modifiers to TrkA endosomes governs retrograde NGF signaling and survival. *Cell*, **146**, 421–434.
47. Coon, B.G., Hernandez, V., Madhivanan, K., Mukherjee, D., Hanna, C.B., Ramirez, I.B., Lowe, M., Beales, P. and Aguilar, R.C. (2012) The Lowe syndrome protein OCRL1 is involved in primary cilia assembly. *Hum. Mol. Gen.*, **21**, 1835–1847.
48. Diao, A., Rahman, D., Pappin, D.J., Lucocq, J. and Lowe, M. (2003) The coiled-coil membrane protein golgin-84 is a novel rab effector required for Golgi ribbon formation. *J. Cell Biol.*, **160**, 201–212.
49. Westerfield, M. (2000) *The Zebrafish Book. A Guide for the Laboratory Use of Zebrafish (*Danio rerio*)*. University of Oregon Press, Eugene, OR.
50. Haud, N., Kara, F., Diekmann, S., Henneke, M., Willer, J.R., Hillwig, M.S., Gregg, R.G., Macintosh, G.C., Gartner, J., Alia, A. *et al.* (2011) rnaset2 mutant zebrafish model familial cystic leukoencephalopathy and reveal a role for RNase T2 in degrading ribosomal RNA. *Proc. Natl Acad. Sci. USA*, **108**, 1099–1103.
51. Jones, D.R., Gonzalez-Garcia, A., Diez, E., Martinez, A.C., Carrera, A.C. and Merida, I. (1999) The identification of phosphatidylinositol 3,5-bisphosphate in T-lymphocytes and its regulation by interleukin-2. *J. Biol. Chem.*, **274**, 18407–18413.
52. Baraban, S.C., Dinday, M.T., Castro, P.A., Chege, S., Guyenet, S. and Taylor, M.R. (2007) A large-scale mutagenesis screen to identify seizure-resistant zebrafish. *Epilepsia*, **48**, 1151–1157.